Spin fluctuations in the ultranodal superconducting state of Fe(Se,S)

Yifu Cao[1], Chandan Setty[2], Andreas Kreisel[3], Laura Fanfarillo[1,4] and P.J. Hirschfeld[1]
[1]*Department of Physics, University of Florida, Gainesville, Florida 32603, USA*
[2]*Department of Physics and Astronomy, Rice Center for Quantum Materials, Rice University, Houston, Texas 77005, USA*
[3]*Niels Bohr Institute, University of Copenhagen, Jagtvej 155 , DK-2200, Copenhagen, Denmark and*
[4]*Istituto dei Sistemi Complessi (ISC-CNR), Via dei Taurini 19, I-00185 Rome, Italy*

The iron-based superconductor FeSe isovalently substituted with S displays an abundance of remarkable phenomena that have not been fully understood, at the center of which are apparent zero-energy excitations in the superconducting state in the tetragonal phase. The phenomenology has been generally consistent with the proposal of the so-called ultranodal states where Bogoliubov Fermi surfaces are present. Recently, nuclear magnetic resonance measurements have seen unusually large upturns in the relaxation rate as temperature decreases to nearly zero in these systems, calling for theoretical investigations. In this paper, we calculate the spin susceptibility of an ultranodal superconductor including correlation effects within the random phase approximation. Although the non-interacting mean-field calculation rarely gives an upturn in the low temperature relaxation rate within our model, we found that correlation strongly enhances scattering between hot spots on the Bogoliubov Fermi surface, resulting in robust upturns when the interaction is strong. Our results suggest that in addition to the presence of Bogoliubov Fermi surfaces, correlation and multiband physics also play important roles in the system's low energy excitations.

I. INTRODUCTION

Iron-based superconductors have been drawing lots of research interest for almost two decades since their discovery, for their relatively high T_c, simple structure and the interplay between rich phenomena including nematicity, magnetization and non-trivial topology[1]. Among all families of iron-based superconductors, the chalcogenide 11 material FeSe has a distinct phase diagram where a nematic transition can occur without accompanying magnetic order[2–7]. The parent compound FeSe shows a nematic transition at around 90K, a superconducting (SC) transition at 9K and no magnetic order under ambient pressure. Upon applying hydrostatic pressure the nematicity is suppressed and antiferromagnetic (AFM) order develops. The AFM order in FeSe under pressure should resemble that observed in iron pnictides, and is likely a stripe order with in-plane magnetic moments [1, 8–10].

On the other hand, the S-substituted FeSe does not show strong evidence for long-ranged magnetic order, but exhibits peculiar changes in its superconducting states across the nematic quantum critical point at around 0.17 sulfur substitution. For $x > 0.17$, the normal state of $FeSe_{1-x}S_x$ is tetragonal, established by various measurements of the electronic structure[2, 11, 12]; and the transport properties show non-Fermi liquid behavior near the quantum critical point[13]. The superconducting state shows curiously large zero energy density of states (DOS), which has so far been evidenced by specific heat and thermal transport measurements[14], scanning tunneling microscopy (STM)[15], angular-resolved photoemission spectroscopy (ARPES)[16] and most recently, by nuclear magnetic resonance (NMR) studies[17].

Possible origins of such residual DOS in the superconducting states of the heavily S-substituted FeSe has been discussed in the aforementioned Ref. [16, 17]. Impurity effects or coexistence of spatially separated SC and normal phase are excluded, because the samples are clean and homogeneous as seen from quantum oscillation[2] and STM experiments[15]. For measurements done under external field such as the NMR measurements, another possible explanation for the observed residual DOS is the Volovik effect[18]. However, the Volovik effect cannot account for the order of magnitude difference in the relaxation rate across samples with different substitution levels but the same external field. It has been suggested[19–21] that the so-called ultranodal superconducting state, which by definition hosts Bogoliubov Fermi surfaces (BFS), is responsible for the large residual DOS in these systems.

Ultranodal states are superconducting states with extended gap nodes that, in contrast to usual point nodes or line nodes in three dimension, have the same dimension as the underlying normal state Fermi surface. Such extended nodes are called Bogoliubov Fermi surfaces[22–24]. The existence of BFS does not necessarily require non-trivial topology, as is the case in [25], but they are topologically protected by a $\mathbb{Z}_2$ invariant if the superconducting state possesses inversion symmetry. In a multiband spin-1/2 superconductor, BFS can arise from a interband non-unitary triplet pairing term or from a magnetic order that breaks time-reversal symmetry, and may[19] or may not[21, 25] preserve the inversion symmetry. It has also been shown[21] that the non-unitarity of the interband triplet pairing can be induced by driving the system close to a magnetic instability, in which case the magnetic moment of the the non-unitary triplet pair aligns with the fluctuating magnetic order.

The existence of a BFS explains well the residual DOS in the tetragonal Fe(Se,S) as seen from specific heat or STS experiments (see however Ref. [26] for an alternative picture), as well as the possible C_4 symmetry breaking in the superconducting phase as seen in the ARPES experiment[16]. However, it has not been fully understood how the ultranodal scenario can fit the recent NMR data presented in Ref. [17].

The NMR measurement in Ref. [17], performed on $FeSe_{1-x}S_x$ at several S-substitution level across the nematic QCP with in-plane applied field and temperature down to 100 mK, shows not only a finite value of $1/(T_1T)$ at zero temperature for the $x = 0.18$ and $x = 0.23$ samples, but also an unusual upturn as temperature decreases to zero. While the former can be understood fairly straightforwardly as yet another signature of the zero energy residual DOS in these materials, the latter requires a more sophisticated understanding. In this paper, we study the models for BFS systems discussed in [19–21] to further calculate the spin fluctuations in the ultranodal states. We compare our calculations of $1/(T_1T)$ to the experimental data, and show that the upturn is likely due to the interplay between strong magnetic fluctuation and multiband physics in such systems.

II. MODEL

We adopt a minimal two-band mean field model with intraband spin-singlet pairing and interband non-unitary spin-triplet pairing from previous works[19–21]

$$H = \sum_{\mathbf{k},\sigma,i} \epsilon_{i\mathbf{k}\sigma} c^\dagger_{i\mathbf{k}\sigma} c_{i\mathbf{k}\sigma} - \sum_{\mathbf{k},i} \Delta_i(\mathbf{k}) (c^\dagger_{i\mathbf{k}\uparrow} c^\dagger_{i-\mathbf{k}\downarrow} + h.c.) - \sum_{\mathbf{k},\sigma} \Delta_{\sigma\sigma}(\mathbf{k}) (c^\dagger_{1\mathbf{k}\sigma} c^\dagger_{2-\mathbf{k}\sigma} + h.c.). \quad (1)$$

Here $i = 1, 2$ is the band index. Seeking qualitative results at low temperatures, we make the assumption that all gaps correspond to a single T_c and follow a BCS-like temperature dependence, where the key feature is that the deviation from the $T = 0$ value is exponentially or power law small at low temperature. Also, for simplicity, we consider a tight-binding model with only nearest neighbor hopping and $\epsilon_{i\mathbf{k}\sigma} = 2(\cos k_x + \cos k_y) - \mu_i$. We have set the nearest neighbor hopping parameter $t = 1$ and adopt it as our unit of energy throughout the calculations below.

We wish to calculate the spin susceptibility

$$\chi^{uv}(\mathbf{q}, t) = -\theta(t) \sum_{\mathbf{q}'} \langle [S^u(\mathbf{q}, t), S^v(\mathbf{q}', 0)] \rangle, \quad (2)$$

where $S^u(\mathbf{q}, t = 0) = \sum_{i,\mathbf{k},\alpha,\beta} c^\dagger_{i\mathbf{k}\alpha} \sigma^u_{\alpha\beta} c_{i\mathbf{k}+\mathbf{q}\beta}$ is the total spin operator summed over the two bands, and $u, v = x, y, z$. In particular, since the z axis of the Pauli matrices denotes the direction of the magnetic moment of our non-unitary triplet pair, which in our model is the direction the magnetization would condense in[21]. We can choose z to be in the crystalline ab plane, i.e. $z \perp c$ corresponding to the direction of the magnetic field in the experiment of Ref. [17], and focus on the zz-component of the spin susceptibility, χ^{zz}.

To this end, we first find the Nambu Green's function $G_\mathbf{k}(\omega)$ by diagonalizing the Nambu Hamiltonian corresponding to Eq. (1). The Nambu basis we use is $\psi_\mathbf{k} = [c_{1\mathbf{k}\uparrow}, c_{1-\mathbf{k}\downarrow}, c_{2-\mathbf{k}\uparrow}, c_{2\mathbf{k}\downarrow}, c^\dagger_{1\mathbf{k}\uparrow}, c^\dagger_{1-\mathbf{k}\downarrow}, c^\dagger_{2-\mathbf{k}\uparrow}, c^\dagger_{2\mathbf{k}\downarrow}]^T$. With the eigenvalues $E_{l\mathbf{k}}$ and the eigenvector matrix $U_\mathbf{k}$ of the Nambu Hamiltonian, the Nambu Green's function can now be expressed as

$$G_\mathbf{k}(\omega) = U^\dagger_\mathbf{k} \mathrm{diag}\left(\frac{1}{\omega - E_{1\mathbf{k}}}, \ \ldots, \ \frac{1}{\omega - E_{8\mathbf{k}}} \right) U_\mathbf{k}. \quad (3)$$

At this point, we would like to also define the 8×8 Nambu spin matrices $\Sigma^u \equiv \mathrm{diag}(\sigma^u, \sigma^u, -(\sigma^u)^T, -(\sigma^u)^T)$, composed of 2×2 Pauli matrices on their diagonal blocks. The bare spin-spin correlation function in the Matsubara representation is $C^{uv}(\mathbf{q}, i\nu) = -\frac{1}{2}\frac{1}{\beta} \sum_{i\omega_n} \sum_\mathbf{k} \mathrm{Tr}\left(\Sigma^u G_{\mathbf{k}+\mathbf{q}}(i\omega_n + i\nu) \Sigma^v G_\mathbf{k}(i\omega_n)\right)$. Substituting in Eq.(3) and having performed the Matsubara sum and the analytic continuation to the real axis, we obtain

$$\chi^{(0)zz}(\mathbf{q}, \omega) = \frac{1}{2} \sum_{l,m} \Sigma^z_{ll} \Sigma^z_{mm} \chi^{(0)}_{llmm}(\mathbf{q}, \omega), \quad (4)$$

where the bare density-density bubble in the quasiparticle band space reads

$$\chi^{(0)}_{llmm}(\mathbf{q}, \omega) = -\sum_{\mathbf{k},r,s} W_{ll}(r\mathbf{k}, s\mathbf{k}+\mathbf{q}) W^*_{mm}(r\mathbf{k}, s\mathbf{k}+\mathbf{q}) \times \frac{f(E_{s\mathbf{k}+\mathbf{q}}) - f(E_{r\mathbf{k}})}{E_{s\mathbf{k}+\mathbf{q}} - E_{r\mathbf{k}} - \omega - i0^+}. \quad (5)$$

Here we defined the coherence factors $W_{ll}(r\mathbf{k}, s\mathbf{k}') \equiv U_{rl\mathbf{k}} U^*_{sl\mathbf{k}'}$, where $r\mathbf{k}$ is a composite label referring to the Bogoliubov quasiparticle at momentum $\mathbf{k}$ in the rth quasiparticle band.

We can further investigate using a random phase approximation (RPA) calculation of the effect of a residual interaction in the particle-hole channel. We consider an interaction of the Hubbard type

$$\begin{aligned} H_U =& \frac{1}{2} \sum_{\mathbf{r},i} U n_{i\mathbf{r}\uparrow} n_{i\mathbf{r}\downarrow} \\ \equiv& \frac{1}{8} \sum_{\mathbf{k},\mathbf{k}',\mathbf{q},l,m} \Gamma_{llmm} \psi^\dagger_{l\mathbf{k}} \psi_{l\mathbf{k}-\mathbf{q}} \psi^\dagger_{m\mathbf{k}'} \psi_{m\mathbf{k}'+\mathbf{q}} \end{aligned} \quad (6)$$

In the last step we have rewritten the interaction using the Nambu basis and defined a coupling tensor Γ that is diagonal in the dimensions labeled by the 1st, 2nd and 3th, 4th indices and a constant function of momentum transfer $\mathbf{q}$. As shown in Appendix, it is sufficient to keep only the partially diagonal part of the full tensor for our purpose of calculating $\chi^{(\mathrm{RPA})zz}$, and both tensors in Eq. (5) and (6) can be treated as 8×8 matrices $\tilde{\chi}^{(0)}_{lm} \equiv \chi^{(0)}_{llmm}$,

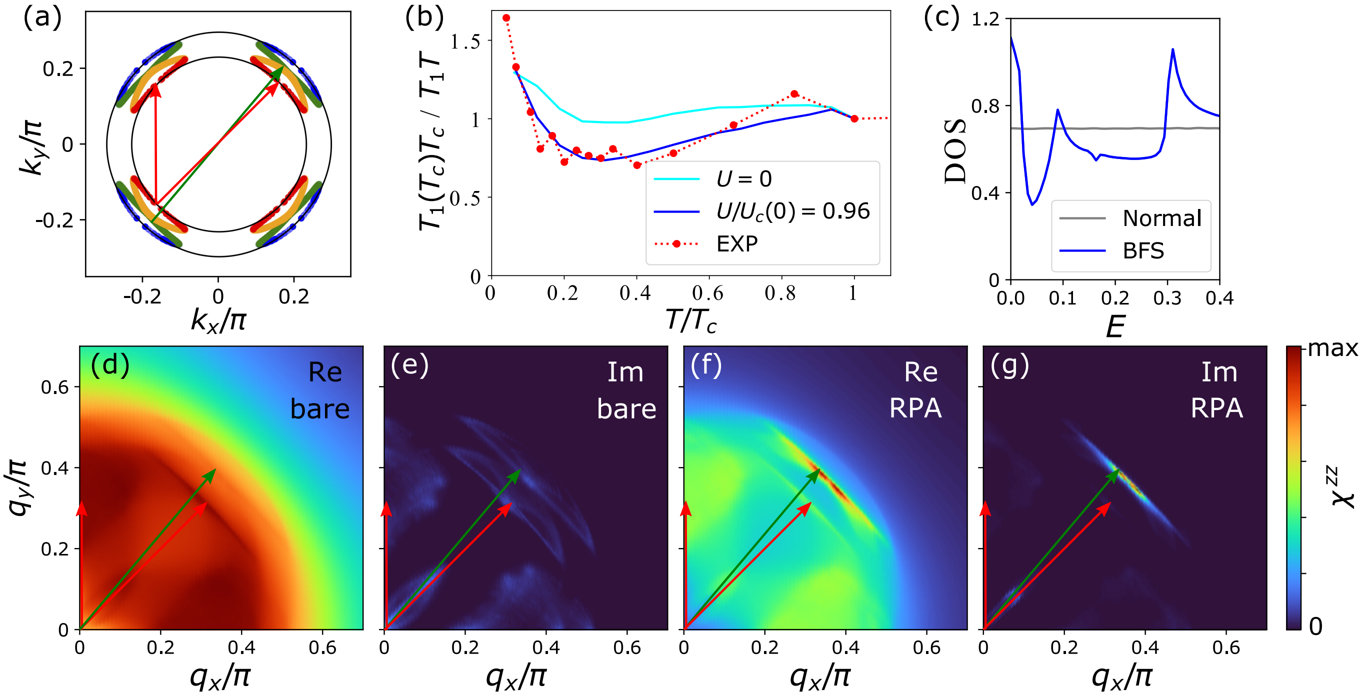

FIG. 1. (a) Normal (black) and Bogoliubov (colored) Fermi surfaces for the two-band model (1), with $\mu_1 = 3.5$, $\mu_2 = 3.2$ and $\Delta_1(\mathbf{k}) = \Delta_2(\mathbf{k}) = 0.06|\cos 2\theta_{\mathbf{k}}|$, where $\theta_{\mathbf{k}}$ is the angle of $\mathbf{k}$ on the 2D Fermi surface. $\Delta_{\uparrow\uparrow}(\mathbf{k}) = 0.15$, $\Delta_{\downarrow\downarrow}(\mathbf{k}) = 0$ at $T = 0$. Within the same color of the BFS the coherent scattering amplitudes are larger than between points on BFSs with different color (See main text Sec. III). Arrows shows some of the dominant scattering processes as seen from panel (d-g). (b)The normalized $1/(T_1T)$ as a function of T below T_c. Cyan and blue curves calculated from bare and RPA susceptibility near a magnetic instability respectively. Red dots are experimental data taken from Ref. [17]. T_c is taken to be 0.08. The critical U is determined from the normal and Bogoliubov band structure, and $U_c(T_c) = 10.8$, $U_c(0) = 9.8$. (c) Zero temperature DOS. (d-g) Real and imaginary parts of the spin susceptibility at $T = 0$. The arrows are the same as in panel (a). One can see that there is a shift of the dominant contribution from the red arrow to green arrow as U increases. The color bar maxima are 0.7, 0.03, 8, 5 for panel (d), (e), (f), (g) respectively.

$\tilde{\Gamma}_{lm} \equiv \Gamma_{llmm}$. The RPA density-density bubble is related to the bare bubble through

$$\tilde{\chi}^{(\mathrm{RPA})}(\mathbf{q},\omega) = \tilde{\chi}^{(0)}(\mathbf{q},\omega)\left(\tilde{I} + \tilde{\Gamma}\tilde{\chi}^{(0)}(\mathbf{q},\omega)\right)^{-1}. \quad (7)$$

The sign convention for the above equation is explained in the appendix. The RPA spin susceptibility is

$$\chi^{(\mathrm{RPA})zz}(\mathbf{q},\omega) = \frac{1}{2}\sum_{l,m}\Sigma^z_{ll}\Sigma^z_{mm}\tilde{\chi}^{(\mathrm{RPA})}_{lm}(\mathbf{q},\omega), \quad (8)$$

by analogy to Eq. (4) with $\chi^{(0)} \to \tilde{\chi}^{(\mathrm{RPA})}$. The NMR relaxation rate probes the spin fluctuation in the system, and is proportional to the imaginary part of the spin susceptibility,

$$\frac{1}{T_1} \propto T \lim_{\omega\to 0}\sum_{\mathbf{q}}\frac{\mathrm{Im}\,\chi^{zz}(\mathbf{q},\omega)}{\omega} \quad (9)$$

III. RESULTS

We numerically calculated the spin susceptibility of the model Hamiltonian BFS. To summarize the result, we found that the bare susceptibility calculation always give rise to non-zero residual $1/(T_1T)$ at zero temperature when BFS are present, as expected due to the zero energy residual DOS. However, the bare $1/(T_1T)$ rarely increases as temperature decrease near $T = 0$, unless van Hove singularities of the Bogoliubov quasiparticle bands are tuned to the Fermi level, contributing to a large zero energy peak in the DOS. On the other hand, if we take into account the correlation effects using the RPA calculation, certain scattering between hot spots on the BFS can get strongly enhanced, resulting in an upturn in the $1/(T_1T)$ as temperature decreases. This can happen when the zero energy DOS is not peaked, or when the BFS are not strongly nested. Below we discuss in details these results.

In Fig 1 and 2 we show in parallel two examples of having upturns in the $1/(T_1T)$ at low temperature as a result of correlations and multiband effects. Fig. 1 corresponds to a scenario where the intraband singlet $\Delta_i(\mathbf{k})$ is taken to be nodal s-wave with accidental nodes along the 45 degree directions, and the interband triplet pairing $\Delta_{\uparrow\uparrow}(\mathbf{k})$ isotropic. Fig. 2 corresponds to the C_2 symmetric scenario discussed in Ref. [21], where the interband

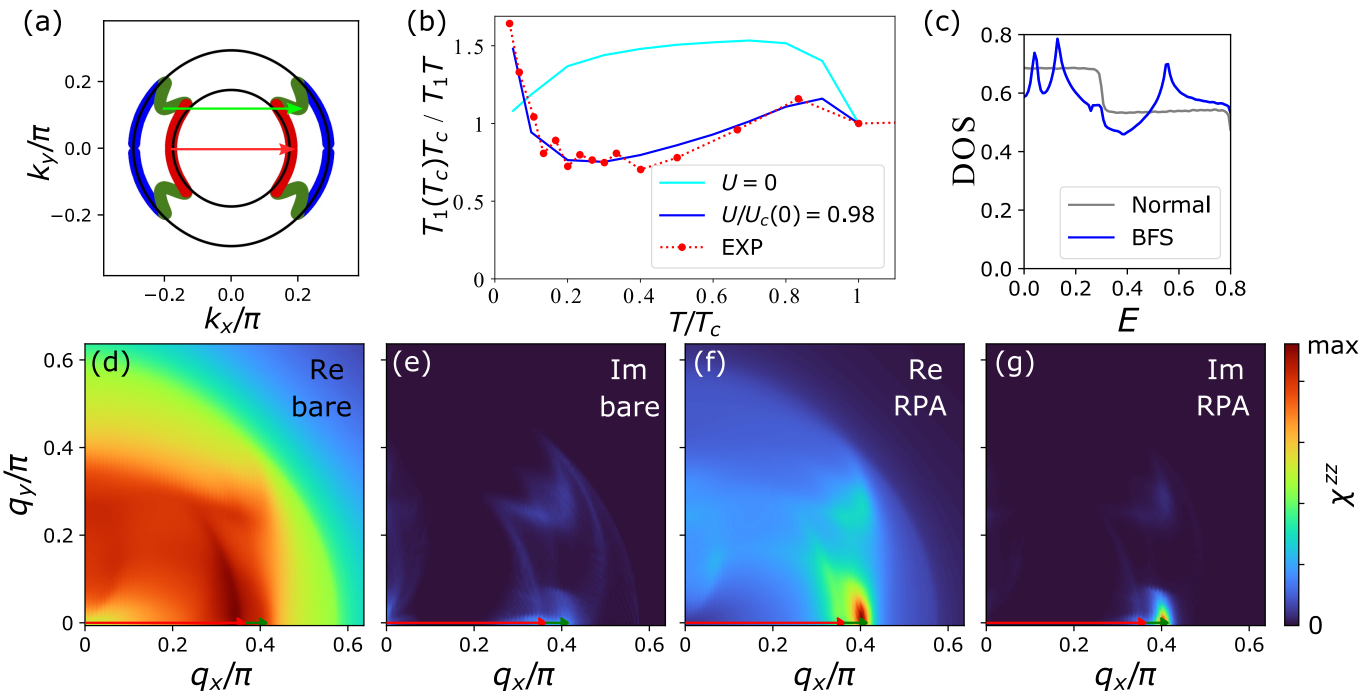

FIG. 2. Same as Fig. 1 but with a different set of parameters: $\mu_1 = 3.7$, $\mu_2 = 3.2$, $\Delta_1(\mathbf{k}) = \Delta_2(\mathbf{k}) = 0.05$, $\Delta_{\uparrow\uparrow}(\mathbf{k}) = 0.3\cos\theta_{\mathbf{k}}$, $\Delta_{\downarrow\downarrow}(\mathbf{k}) = 0$, $T_c = 0.1$. $U_c(T_c) = 10.8$, $U_c(0) = 10$. The color bar maxima are 0.7, 0.026, 15, 2.3 for panel (d), (e), (f), (g) respectively.

triplet pairing $\Delta_{\uparrow\uparrow}(\mathbf{k})$ is assumed to be p-wave and the intraband singlet pairing $\Delta_i(\mathbf{k})$ is taken to be isotropic for simplicity. A BFS then forms only when $\Delta_{\uparrow\uparrow}$ is sufficiently large.

In both cases we have set $\Delta_{\downarrow\downarrow}(\mathbf{k}) = 0$. In Fig. 1, the bare susceptibility already gives rise to an upturn in the $1/(T_1T)$ (panel (b) cyan curve). This is because the van Hove singularity (band extremum corresponding to where the superconducting gap opens) of the Bogoliubov band has been tuned at the Fermi level by changing the interband order parameter, and a peak in the quasiparticle density of states exists at exactly zero energy (panel (c)). We found that upturns in the bare $1/(T_1T)$ at low temperature seem to be always associated with such peaks at zero energy in the DOS. Although such peaks in the DOS are not desired as they are not consistent with the spectroscopic data[15], they are not required once we include correlations. This can be seen in Fig. 2 (b) and (c), where the density of states is not peaked at zero energy and the bare $1/(T_1T)$ curve does not have an upturn while the RPA curve close to magnetic instability does. The qualitative difference between the $U = 0$ curve and the $U \lessapprox U_c(0)$ curve in Fig. 2 (b) is unusual, since normally one would expect, from its simplest form for the normal metal as in Eq. (A.13), the RPA susceptibility to be enhanced further where the bare susceptibility is already large.

To better understand this unusual behavior, we first divide the BFS into several segments, as shown by the color scheme in panel (a) of Fig. 1 and 2, within each segment the scattering is much stronger than across different segments. This is done by treating the $\mathbf{k}$-points on the BFS as vertices of an weighted undirected graphs with weights given by the coherence factors defined in Eq. (5), and employing the Leiden algorithm for community detection[27, 28]. We see that the parts of the BFS that follow the shape of the normal Fermi surfaces (red and blue in panel (a)) are well separated from the rest of the BFSs in terms of scattering processes. Then in panel (d,e) we plot the bare spin susceptibility as in Eq. (4) at zero temperature, and in panel (f,g) we show the RPA spin susceptibility (8) at $U \lessapprox U_c(0)$ and zero temperature. We identify the important $\mathbf{q}$ vectors as the red and green arrows connecting segments of BFSs with the same color shown in Fig. 2(a). From panel (d) we see that the real part of the bare susceptibility is the largest at the $\mathbf{q}$ vectors connecting the red part of the BFSs, but is not strongly peaked at any particular $\mathbf{q}$ vector. The latter observation is an indication of no strong nesting between the the BFSs. Secondly, by comparing panel (d,e) with panel (f,g), we see that although the $\mathbf{q}$ vectors that connect the green part of the BFSs are only subdominant in the bare susceptibility, they become the dominant $\mathbf{q}$ vectors that connect "hot spots" on the BFSs near the magnetic instability. This shift of the dominant $\mathbf{q}$ vectors as the interaction U increases within an RPA calculation can only be explained by nontrivial multiband effects embedded in the coherence factor W, which is consistent with the unusual change in the shape of the normalized $1/(T_1T)$ curve as U increases.

IV. CONCLUSION

To summarize, we have calculated the spin susceptibilities for the ultranodal states in a minimal two-band model, where the interband non-unitary spin-triplet pairing is responsible for the Bogoliubov Fermi surfaces. We found that the existence of BFSs in such models naturally gives rise to finite residual value in the $1/T_1T$ at zero temperature, but does not necessarily produce the large upturns at low temperature, as seen in the experiments [17] on the Fe(Se,S) system, in a non-interacting calculation. We then studied the effect of correlation within random phase approximation in the ultranodal state. By adding a Hubbard interaction in the particle-hole channel while not changing the pre-assumed pairing gaps, we see that the spin susceptibilities at $\mathbf{q}$ vectors connecting hot spots on the BFS get strongly enhanced at low temperature when the interaction is strong, resulting in upturns in $1/T_1T$ irrespective of the presence or absence of upturns in the bare calculation. The hot spots have strong interband character as indicated from their position on the BFSs, and do not have particularly large contribution to the spin susceptibilities at weak interaction. Therefore, we conclude the experimentally observed upturn in $1/T_1T$ can be explained as a combined effect of the presence of BFS, interband physics and correlation.

Our theory is primarily applicable to the tetragonal phase of $\mathrm{FeSe}_{1-x}\mathrm{S}_x$ with $x > 0.17$ at ambient pressure. For the nematic phase with $x < 0.17$ at ambient pressure and the tetragonal phase with $x < 0.17$ under pressure[29], the low temperature $1/T_1T$ seems to have a Korringa behavior, i.e. constant in temperature, with smaller but finite residual values. Our calculation of the $1/T_1T$ is consistent with these data assuming weak correlation or small BFSs, but whether the ultranodal scenario can apply to these situations requires a more careful and comprehensive study in the future.

V. ACKNOWLEDGEMENTS

L. F. acknowledges support by the European Union's Horizon 2020 research and innovation programme through the Marie Skłodowska-Curie grant SuperCoop (Grant No 838526). P.J.H. and Y.C. were supported by DOE grant number DE-FG02-05ER46236. A.K. acknowledges support by the Danish National Committee for Research Infrastructure (NUFI) through the ESS-Lighthouse Q-MAT.

APPENDIX

In this appendix we provide information about our sign convention in Eq. (7), and how the standard multiorbital RPA formalism in e.g. Ref. [30, 31] corresponds to our 8×8 matrix formalism in Nambu space. We start by considering a bare bubble that is Eq. (5) in its general form

$$\chi^{(0)}_{ll'mm'}(\mathbf{q},\omega) = -\sum_{\mathbf{k},r,s} U_{rl\mathbf{k}} U^*_{sl'\mathbf{k+q}} U^*_{rm\mathbf{k}} U_{sm'\mathbf{k+q}} \frac{f(E_{s\mathbf{k+q}}) - f(E_{r\mathbf{k}})}{E_{s\mathbf{k+q}} - E_{r\mathbf{k}} - \omega - i0^+} \tag{A.1}$$

It transforms like a $8 \times 8 \times 8 \times 8$ rank-4 tensor as the Numbu basis transforms, while contracts like a 64×64 rank-2 tensor (matrix with ll' a composite row index and mm' a composite column index) in the RPA series. Accordingly the full coupling tensor corresponding to the Hubbard interaction in Eq. (6) can be redefined as

$$H_U = \frac{1}{2}\sum_{\mathbf{r},i} U n_{i\mathbf{r}\uparrow} n_{i\mathbf{r}\downarrow} = \frac{1}{16}\sum_{\mathbf{k},\mathbf{k}',\mathbf{q},l,m,l',m'} \Gamma_{l l' m m'} \psi^\dagger_{l\mathbf{k}} \psi_{l'\mathbf{k-q}} \psi^\dagger_{m\mathbf{k}'} \psi_{m'\mathbf{k'+q}} \tag{A.2}$$

where on the RHS the terms quadratic in c,$c^\dagger$ has been discarded since they only renormalize the chemical potential. Let's represent $\Gamma_{ll'mm'}$ as a 64×64 matrix which only has two 8×8 non-zero blocks, ordered as following:

$$[\Gamma_{ll'mm'}]_{64\times 64} = \begin{pmatrix} [\Gamma_{llmm}]_{8\times8} & 0_{8\times48} & 0_{8\times8} \\ 0_{48\times8} & 0_{48\times48} & 0_{8\times48} \\ 0_{8\times8} & 0_{8\times48} & [\Gamma_{l\bar{l}m\bar{m}}]_{8\times8} \end{pmatrix} \tag{A.3}$$

The first 8×8 block $[\Gamma_{llmm}]$ is the same as the $\tilde{\Gamma}$ in Eq. (6), and is the direct interaction. The other 8×8 block $[\Gamma_{l\bar{l}m\bar{m}}]$ is the exchange interaction. Here $\bar{l}$ is defined as the the Nambu index that corresponds to the time-reversed lth operator in the Nambu basis. For example, $\bar{1} = 2$ and $\bar{8} = 7$ (c.f. the choice of our Nambu basis above Eq. (3)). The matrix elements of $[\Gamma_{llmm}]$ and $[\Gamma_{l\bar{l}m\bar{m}}]$ are tabulated as in Table I.

To calculate the χ^{zz} component of the spin susceptibility, we can write the Σ^z operator (defined in the main text below Eq. (3)) as a 1×64 vector, which in the same basis as for Eq. (A.3) is

$$[\Sigma^z_{ll'}]_{1\times64} = (\mathrm{diag}(\Sigma^z), 0_{1\times48}, 0_{1\times8}) \tag{A.4}$$

ll' \ mm'	11	22	33	44	55	66	77	88
11	0	U	0	0	0	0	0	0
22	U	0	0	0	0	0	0	0
33	0	0	0	U	0	0	0	0
44	0	0	U	0	0	0	0	0
55	0	0	0	0	0	U	0	0
66	0	0	0	0	U	0	0	0
77	0	0	0	0	0	0	0	U
88	0	0	0	0	0	0	U	0

ll' \ mm'	12	21	34	43	56	65	78	87
12	0	-U	0	0	0	0	0	0
21	-U	0	0	0	0	0	0	0
34	0	0	0	-U	0	0	0	0
43	0	0	-U	0	0	0	0	0
56	0	0	0	0	0	-U	0	0
65	0	0	0	0	-U	0	0	0
78	0	0	0	0	0	0	0	-U
87	0	0	0	0	0	0	-U	0

TABLE I. Non-zero matrix elements of $[\Gamma_{ll'mm'}]$. The left panel corresponds to the 8×8 block $[\Gamma_{llmm}]$ in Eq.(A.3), and the right panel corresponds to the 8×8 block $[\Gamma_{l\bar{l}m\bar{m}}]$.

The RPA spin susceptibility then is

$$\chi^{(\mathrm{RPA})zz}(\mathbf{q},\omega)=\frac{1}{2}[\Sigma^z][\chi^{(0)}](\mathbf{q},\omega)\left(I_{64\times 64}+[\Gamma][\chi^{(0)}](\mathbf{q},\omega)\right)^{-1}[\Sigma^z]^T \tag{A.5}$$

We want to show that Eq. (A.5) is equivalent to Eq. (7) and (8) where the tilded matrices are essentially the first 8×8 blocks of the $[\cdot]$ matrices. Since the vector $[\Sigma^z]$ bears the form of Eq. (A.4), it suffices to show that

$$[\chi^{(0)}](\mathbf{q},\omega)\left(I_{64\times 64}+[\Gamma][\chi^{(0)}](\mathbf{q},\omega)\right)^{-1}=\begin{pmatrix}\tilde{\chi}^{(\mathrm{RPA})}(\mathbf{q},\omega) & * & * \\ * & * & * \\ * & * & *\end{pmatrix} \tag{A.6}$$

where $\tilde{\chi}^{(\mathrm{RPA})}(\mathbf{q},\omega)$ is the 8×8 matrix defined in Eq. (7), and $*$'s are placeholders for unimportant blocks. Since $[\Gamma]$ has the form of Eq. (A.3), without using any knowledge about $[\chi^{(0)}]$ except that the first 8×8 block of it is $\tilde{\chi}^{(0)}$, we can see that $I_{64\times 64}+[\Gamma][\chi^{(0)}](\mathbf{q},\omega)$ should have the following form

$$I_{64\times 64}+[\Gamma][\chi^{(0)}](\mathbf{q},\omega)=\begin{pmatrix}\tilde{I}+\tilde{\Gamma}\tilde{\chi}^{(0)}(\mathbf{q},\omega) & B_{8\times 48} & C_{8\times 8} \\ 0_{48\times 8} & I_{48\times 48} & 0_{48\times 8} \\ D_{8\times 8} & E_{8\times 48} & F_{8\times 8}\end{pmatrix} \tag{A.7}$$

Its inverse can be calculated as

$$\left(I_{64\times 64}+[\Gamma][\chi^{(0)}](\mathbf{q},\omega)\right)^{-1}=\begin{pmatrix}A^{-1}+A^{-1}C(F-DA^{-1}C)^{-1}DA^{-1} & * & * \\ 0 & * & * \\ * & * & *\end{pmatrix} \tag{A.8}$$

where we have denoted $A\equiv\tilde{I}+\tilde{\Gamma}\tilde{\chi}^{(0)}(\mathbf{q},\omega)$. Now if we take a close look at the structure of $[\chi^{(0)}]$, we will see that it is zero at the off-diagonal block $\chi^{(0)}_{llm\bar{m}}$, namely

$$[\chi^{(0)}](\mathbf{q},\omega)=\begin{pmatrix}\tilde{\chi}^{(0)}(\mathbf{q},\omega) & * & 0_{8\times 8} \\ * & * & * \\ 0_{8\times 8} & * & [\chi^{(0)}_{l\bar{l}m\bar{m}}]_{8\times 8}\end{pmatrix} \tag{A.9}$$

This is because the pair of Green's functions $G_{\bar{m}l\mathbf{k}}(\omega')$ and $G_{lm\mathbf{k}+\mathbf{q}}(\omega'+\omega)$ cannot be both non-zero at the same time given that there is only the intraband singlet pairing and interband triplet pairing processes in the Hamltonian (1). Now if we combine Eq. (A.8) and (A.9) and notice that $C=D=0$ once we know (A.9), we see that Eq. (A.6) is true. Therefore, we have shown that the full RPA treatment of our model can be reduced to an 8×8 matrix formalism, which is easier to deal with numerically.

As a further sanity check, we turn off the pairing amplitudes and calculate the charge and spin susceptibility in the normal state starting from Eq. (7). In this case $\tilde{\chi}^{(0)}(\mathbf{q},\omega)$ is a diagonal matrix, and $\tilde{\Gamma}\tilde{\chi}^{(0)}(\mathbf{q},\omega)$ is block diagonal with four 2×2 blocks on the diagonal. Let's take the first block as an example (for a one band system) and denote the 2×2 matrices as hatted matrices and the matrix elements $\chi^{(0)}_{1111}=\chi^{(0)}_{2222}\equiv\chi^{(0)}_1$. We have

$$\hat{I}+\hat{\Gamma}\hat{\chi}^{(0)}(\mathbf{q},\omega)=\begin{pmatrix}1 & U\chi^{(0)}_1(\mathbf{q},\omega) \\ U\chi^{(0)}_1(\mathbf{q},\omega) & 1\end{pmatrix} \tag{A.10}$$

Inverting the above matrix gives

$$\hat{\chi}^{(\mathrm{RPA})}(\mathbf{q},\omega) = \hat{\chi}^{(0)}(\mathbf{q},\omega)\left(\hat{I} + \hat{\Gamma}\hat{\chi}^{(0)}(\mathbf{q},\omega)\right)^{-1} = \frac{\chi_1^{(0)}(\mathbf{q},\omega)}{1 - U^2\chi_1^{(0)}(\mathbf{q},\omega)^2}\begin{pmatrix} 1 & -U\chi_1^{(0)}(\mathbf{q},\omega) \\ -U\chi_1^{(0)}(\mathbf{q},\omega) & 1 \end{pmatrix} \tag{A.11}$$

The diagonal elements $\chi_{1111}^{(\mathrm{RPA})}(\mathbf{q},\omega) = \chi_{2222}^{(\mathrm{RPA})}(\mathbf{q},\omega)$ are the polarization bubbles with the same spin on the left and right vertices (Here 1 stands for up and 2 stands for down, c.f. the choice of our Nambu basis above Eq. (3)). The off-diagonal elements are the bubble with opposite spins on the vertices. The charge susceptibility of the first band is given by

$$\chi^{(\mathrm{RPA})c}(\mathbf{q},\omega) = \chi_{1111}^{(\mathrm{RPA})} + \chi_{1122}^{(\mathrm{RPA})} + \chi_{2211}^{(\mathrm{RPA})} + \chi_{2222}^{(\mathrm{RPA})} = \frac{2\chi_1^{(0)}(\mathbf{q},\omega)}{1 + U\chi_1^{(0)}(\mathbf{q},\omega)} \tag{A.12}$$

And the spin susceptibility of the first band is

$$\chi^{(\mathrm{RPA})zz}(\mathbf{q},\omega) = \chi_{1111}^{(\mathrm{RPA})} - \chi_{1122}^{(\mathrm{RPA})} - \chi_{2211}^{(\mathrm{RPA})} + \chi_{2222}^{(\mathrm{RPA})} = \frac{2\chi_1^{(0)}(\mathbf{q},\omega)}{1 - U\chi_1^{(0)}(\mathbf{q},\omega)} \tag{A.13}$$

[1] R. Fernandes, A. Coldea, H. Ding, I. Fisher, P. Hirschfeld, and G. Kotliar, Iron pnictides and chalcogenides: a new paradigm for superconductivity, Nature **601**, 35 (2022).

[2] A. I. Coldea, S. F. Blake, S. Kasahara, A. A. Haghighirad, M. D. Watson, W. Knafo, E. S. Choi, A. McCollam, P. Reiss, T. Yamashita, M. Bruma, S. C. Speller, Y. Matsuda, T. Wolf, T. Shibauchi, and A. J. Schofield, Evolution of the low-temperature fermi surface of superconducting $FeSe_{1-x}S_x$ across a nematic phase transition, npj Quantum Materials **4**, 2 (2019).

[3] A. Kreisel, P. J. Hirschfeld, and B. M. Andersen, On the Remarkable Superconductivity of FeSe and Its Close Cousins, Symmetry **12**, 1402 (2020).

[4] J. Sun, K. Matsuura, G. Ye, Y. Mizukami, M. Shimozawa, K. Matsubayashi, M. Yamashita, T. Watashige, S. Kasahara, Y. Matsuda, J. Yan, B. Sales, Y. Uwatoko, J. Cheng, and T. Shibauchi, Dome-shaped magnetic order competing with high-temperature superconductivity at high pressures in FeSe, Nature communications **7**, 12146 (2016).

[5] K. Matsuura, Y. Mizukami, Y. Arai, Y. Sugimura, N. Maejima, A. Machida, T. Watanuki, T. Fukuda, T. Yajima, Z. Hiroi, K. Y. Yip, Y. C. Chan, Q. Niu, S. Hosoi, K. Ishida, K. Mukasa, S. Kasahara, J.-G. Cheng, S. K. Goh, Y. Matsuda, Y. Uwatoko, and T. Shibauchi, Maximizing T_c by tuning nematicity and magnetism in $FeSe_{1-x}S_x$ superconductors, Nature Communications **8**, 1143 (2017).

[6] M. Bendele, A. Amato, K. Conder, M. Elender, H. Keller, H.-H. Klauss, H. Luetkens, E. Pomjakushina, A. Raselli, and R. Khasanov, Pressure induced static magnetic order in superconducting $FeSe_{1-x}$, Phys. Rev. Lett. **104**, 087003 (2010).

[7] T. Terashima, N. Kikugawa, S. Kasahara, T. Watashige, T. Shibauchi, Y. Matsuda, T. Wolf, A. E. Böhmer, F. Hardy, C. Meingast, H. v. Löhneysen, and S. Uji, Pressure-induced antiferromagnetic transition and phase diagram in FeSe, Journal of the Physical Society of Japan **84**, 063701 (2015).

[8] P. S. Wang, S. S. Sun, Y. Cui, W. H. Song, T. R. Li, R. Yu, H. Lei, and W. Yu, Pressure induced stripe-order antiferromagnetism and first-order phase transition in FeSe, Phys. Rev. Lett. **117**, 237001 (2016).

[9] C. de la Cruz, Q. Huang, J. W. Lynn, J. Li, W. R. II, J. L. Zarestky, H. A. Mook, G. F. Chen, J. L. Luo, N. L. Wang, and P. Dai, Magnetic order close to superconductivity in the iron-based layered $LaO_{1-x}F_xFeAs$ systems, Nature **453**, 899 (2008).

[10] R. Stadel, D. D. Khalyavin, P. Manuel, K. Yokoyama, S. Lapidus, M. H. Christensen, R. M. Fernandes, D. Phelan, D. Y. Chung, R. Osborn, S. Rosenkranz, and O. Chmaissem, Multiple magnetic orders in $LaFeAs_{1-x}P_xO$ uncover universality of iron-pnictide superconductors, Communications Physics **5**, 146 (2022).

[11] A. I. Coldea, Electronic nematic states tuned by isoelectronic substitution in bulk $FeSe_{1-x}S_x$, Frontiers in Physics **8**, 10.3389/fphy.2020.594500 (2021).

[12] P. Reiss, M. D. Watson, T. K. Kim, A. A. Haghighirad, D. N. Woodruff, M. Bruma, S. J. Clarke, and A. I. Coldea, Suppression of electronic correlations by chemical pressure from FeSe to FeS, Phys. Rev. B **96**, 121103(R) (2017).

[13] S. Licciardello, J. Buhot, J. Lu, J. Ayres, S. Kasahara, Y. Matsuda, T. Shibauchi, and N. E. Hussey, Electrical resistivity across a nematic quantum critical point, Nature **567**, 213 (2019).

[14] Y. Sato, S. Kasahara, T. Taniguchi, X. Xing, Y. Kasahara, Y. Tokiwa, Y. Yamakawa, H. Kontani, T. Shibauchi, and Y. Matsuda, Abrupt change of the superconducting gap structure at the nematic critical point in $FeSe_{1-x}S_x$, Proceedings of the National Academy of Sciences **115**, 1227 (2018).

[15] T. Hanaguri, K. Iwaya, Y. Kohsaka, T. Machida,

T. Watashige, S. Kasahara, T. Shibauchi, and Y. Matsuda, Two distinct superconducting pairing states divided by the nematic end point in $FeSe_{1-x}S_x$, Science Advances **4**, eaar6419 (2018).
[16] T. Nagashima, T. Hashimoto, S. Najafzadeh, S.-i. Ouchi, T. Suzuki, A. Fukushima, S. Kasahara, K. Matsuura, M. Qiu, Y. Mizukami, *et al.*, Discovery of nematic Bogoliubov Fermi surface in an iron-chalcogenide superconductor, preprint 10.21203/rs.3.rs-2224728/v1 (2022).
[17] Z. Yu, K. Nakamura, K. Inomata, X. Shen, T. Mikuri, K. Matsuura, Y. Mizukami, S. Kasahara, Y. Matsuda, T. Shibauchi, Y. Uwatoko, and N. Fujiwara, Spin fluctuations from Bogoliubov Fermi surfaces in the superconducting state of S-substituted FeSe, Communications Physics **6**, 175 (2023).
[18] Y. Bang, Volovik effect on nmr measurements of unconventional superconductors, Phys. Rev. B **85**, 104524 (2012).
[19] C. Setty, S. Bhattacharyya, Y. Cao, A. Kreisel, and P. J. Hirschfeld, Topological ultranodal pair states in iron-based superconductors, Nature Communications **11**, 523 (2020).
[20] C. Setty, Y. Cao, A. Kreisel, S. Bhattacharyya, and P. J. Hirschfeld, Bogoliubov Fermi surfaces in spin-$\frac{1}{2}$ systems: Model Hamiltonians and experimental consequences, Phys. Rev. B **102**, 064504 (2020).
[21] Y. Cao, C. Setty, L. Fanfarillo, A. Kreisel, and P. J. Hirschfeld, Microscopic origin of ultranodal superconducting states in spin-$\frac{1}{2}$ systems, Phys. Rev. B **108**, 224506 (2023).
[22] D. F. Agterberg, P. M. R. Brydon, and C. Timm, Bogoliubov Fermi surfaces in superconductors with broken time-reversal symmetry, Phys. Rev. Lett. **118**, 127001 (2017).
[23] C. Timm, A. P. Schnyder, D. F. Agterberg, and P. M. R. Brydon, Inflated nodes and surface states in superconducting half-Heusler compounds, Phys. Rev. B **96**, 094526 (2017).
[24] P. M. R. Brydon, D. F. Agterberg, H. Menke, and C. Timm, Bogoliubov Fermi surfaces: General theory, magnetic order, and topology, Phys. Rev. B **98**, 224509 (2018).
[25] H. Wu, A. Amin, Y. Yu, and D. F. Agterberg, Nematic bogoliubov fermi surfaces from magnetic toroidal order in $FeSe_{1-x}S_x$ (2023), arXiv:2306.11200 [cond-mat.supr-con].
[26] K. Ranjibul Islam and A. Chubukov, Unconventional Superconductivity near a Nematic Instability in a Multi-Orbital system, arXiv e-prints , arXiv:2310.17728 (2023), arXiv:2310.17728 [cond-mat.supr-con].
[27] V. A. Traag, L. Waltman, and N. J. Van Eck, From louvain to leiden: guaranteeing well-connected communities, Scientific reports **9**, 5233 (2019).
[28] G. Csardi, T. Nepusz, *et al.*, The igraph software package for complex network research, InterJournal, complex systems **1695**, 1 (2006).
[29] K. Rana, L. Xiang, P. Wiecki, R. A. Ribeiro, G. G. Lesseux, A. E. Böhmer, S. L. Bud'ko, P. C. Canfield, and Y. Furukawa, Impact of nematicity on the relationship between antiferromagnetic fluctuations and superconductivity in $FeSe_{0.91}S_{0.09}$ under pressure, Phys. Rev. B **101**, 180503 (2020).
[30] A. T. Rømer, D. D. Scherer, I. M. Eremin, P. J. Hirschfeld, and B. M. Andersen, Knight shift and leading superconducting instability from spin fluctuations in Sr_2RuO_4, Phys. Rev. Lett. **123**, 247001 (2019).
[31] A. T. Rømer, T. A. Maier, A. Kreisel, P. J. Hirschfeld, and B. M. Andersen, Leading superconducting instabilities in three-dimensional models for sr_2ruo_4, Phys. Rev. Res. **4**, 033011 (2022).